International Journal of Advanced Robotic Systems

6-REXOS: Upper Limb Exoskeleton Robot with Improved pHRI

Regular Paper

Malin Gunasekara[1]*, Ruwan Gopura[1] and Sanath Jayawardena[1]

1 University of Moratuwa, Katubedda, Sri Lanka
*Corresponding author(s) E-mail: malingunasekara@gmail.com

Received 02 November 2014; Accepted 30 January 2015

DOI: 10.5772/60440

Abstract

Close interaction can be observed between an exoskeleton robot and its wearer. Therefore, appropriate physical human-robot interaction (pHRI) should be considered when designing an exoskeleton robot to provide safe and comfortable motion assistance. Different features have been used in recent studies to enhance the pHRI in upper-limb exoskeleton robots. However, less attention has been given to integrating kinematic redundancy into upper-limb exoskeleton robots to improve the pHRI. In this context, this paper proposes a six-degrees-of-freedom (DoF) upper-limb exoskeleton robot (6-REXOS) for the motion assistance of physically weak individuals. The 6-REXOS uses a kinematically different structure to that of the human lower arm, where the exoskeleton robot is worn. The 6-REXOS has four active DoFs to generate the motion of the human lower arm. Furthermore, two flexible bellow couplings are attached to the wrist and elbow joints to generate two passive DoFs. These couplings not only allow translational motion in wrist and elbow joints but also a redundancy in the robot. Furthermore, the compliance of the flexible coupling contributes to avoiding misalignments between human and robot joint axes. The redundancy in the 6-REXOS is verified based on manipulability index, minimum singular value, condition number and manipulability ellipsoids. The 6-REXOS and a four-DoF exoskeleton robot are compared to verify the manipulation advantage due to the redundancy. The four-DoF exoskeleton robot is designed by excluding the two passive DoFs of the 6-REXOS. In addition, a kinematic model is proposed for the human lower arm to validate the performance of the 6-REXOS. Kinematic analysis and simulations are carried out to validate the 6-REXOS and human-lower-arm model.

Keywords exoskeleton robot, pHRI, redundancy, compliance, manipulability index

1. Introduction

Number of DoF used in recent upper-limb exoskeleton robots is made to match the adjacent human-upper-limb [1]. In the present context, exoskeleton robots are used for rehabilitation, motion assistance, power augmentation and haptic interaction for virtual reality [2]. Unlike with industrial robots, the robot wearer is a significant element in an exoskeleton robot system. Typically, the interaction between the wearer and the exoskeleton robot is twofold [3]. One interaction is called physical human-robot interaction (pHRI) which necessitates the suitability of the exoskeleton structure for the wearer [3]. Cognitive human-robot interaction (cHRI) is the other interaction, which takes intelligence into account for the control of the robot [3]. In order to provide safe and comfortable upper-limb

motions, pHRI has a more significant role than cHRI. Furthermore, different aspects such as weight, actuation, power transmission, dexterity, singularity, workspace, kinematic chain, DoF, and compliance are important aspects under pHRI [3]. Two different directions under cHRI are addressed in recent upper-limb exoskeleton robots: neuro-fuzzy compliance control [4] and neuro-fuzzy control with force vectors [5]. Nevertheless, only a few instances are reported in the literature where pHRI is specifically addressed: low robot weight structure [6] and open arm configuration for forearm [7]. DoF is an important aspect under pHRI [3]. Kinematic matching between the exoskeleton robot and the human limb to which the robot is attached is a common feature in recent exoskeleton robots. As the human upper limb has seven DoFs [8], several upper-limb exoskeleton robots use seven DoFs in their kinematic chain, for example CARDEN-7 [2] and SUEFUL-7 [9]. In general, six DoFs are required to achieve desired position and orientation in 3D space. Due to the availability of additional DoFs, the human upper limb can be considered the best example of a natural redundant manipulator [10]. Because of redundancy, the human upper limb shows higher dexterity in manipulation and greater ability to avoid obstacles and minimum singularities [11]. To improve the pHRI for comfort and ease of manipulation, kinematically different structures (see Fig.1 [3]) are rarely explored in the recent literature [3]. Quantitative analysis to identify the effectiveness of such exoskeleton robots is also rare.

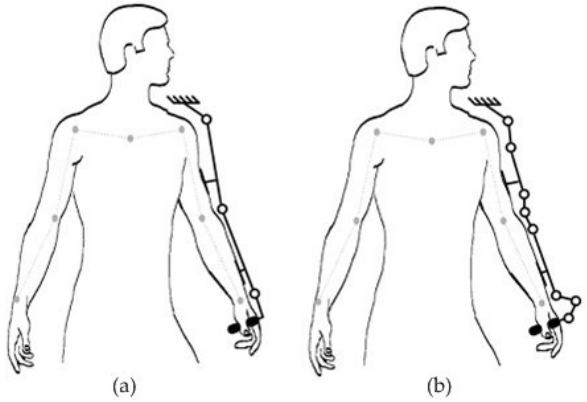

Figure 1. (a) Exoskeleton with fewer DoFs than human limb; (b) exoskeleton with more DoFs than human limb

The human upper limb has a complex and flexible anatomical structure. The instantaneous centres of rotation (ICR) at elbow and shoulder joints change with the joint motion [3]. Such changes pose challenges in the design of an upper-limb exoskeleton robot. Furthermore, misalignments between human and robot joint axes can also occur as a result of ignoring the motion of ICR in the exoskeleton robot [12]. As a result, high reactive forces and torques can be generated at connecting points. Factually, the comfortable range of pressure at interactive points between human and robot is 10-30 mmHg [13]. If such joint axes misalignment is neglected it leads to a high cognitive load as well as a high contact pressure. This pressure creates discomfort to the wearer and degrades the pHRI of the exoskeleton robot. Different techniques are used in upper-limb exoskeleton robots to minimize the effect of joint axes misalignment. A cable drive system is proposed in MEDARM to overcome the effect of ICR motion at the shoulder [14]. Motion of centre of rotation (CR) is considered in the design proposed in [15]. A compliant actuation system is used in NEUROExos to avoid joint axes misalignment at the elbow joint [16]. In many cases, complex mechanisms are proposed to overcome the effect of joint axes misalignment in exoskeleton robots. These may cause an increase in the weight of the exoskeleton robot; an extended structure can also hinder the ability to perform daily activities with the exoskeleton robot [17]. In particular, the compliance can be used to improve the safety, comfort and reliability [18] in robotic applications. These are fundamental requirements of pHRI in exoskeleton robots. Furthermore, compliance can effectively be applied to minimize kinematic discrepancies in exoskeleton robots [19]. However, upper-limb exoskeleton robots with compliance and kinematic redundancy are rarely explored in the literature. Compliance is achieved in many exoskeleton robots using mechanisms which do not alter the DoFs. Furthermore, unless the DoFs are not modified, kinematic performances of the exoskeleton robot such as dexterous manipulation cannot be improved.

This paper proposes a six-DoF upper-limb exoskeleton robot (6-REXOS) which supports elbow flexion-extension, forearm supination-pronation, wrist flexion-extension and wrist ulnar-radial deviation. The 6-REXOS has four active rotational DoFs and two passive translational DoFs, i.e., more than are available in the human lower arm. Two passive DoFs are connected in the wrist and elbow joints to keep their axes parallel to each other. This configuration allows kinematic redundancy of the exoskeleton robot. Moreover, two passive DoFs are attached to the 6-REXOS by means of flexible bellow coupling [20]. Other than redundancy, the 6-REXOS uses several measures to improve the pHRI, for example passive compliance of the bellow coupling. Achieving redundancy as well as compliance in the 6-REXOS is a novel design approach. Redundancy in the 6-REXOS is analysed based on dexterity measures such as manipulability index, minimum singular value, condition number and manipulability ellipsoids. The redundancy of the 6-REXOS is verified by comparing kinematic measures of a four-DoF kinematic chain, which is derived from excluding the two passive DoF in the 6-REXOS. Furthermore, a kinematic model is proposed for the human lower arm. A manipulability measure of the human kinematic model is used to verify the effectiveness of the kinematic redundancy of the 6-REXOS. The significance of the compliance at the wrist joint of the 6-REXOS is investigated using the manipulability measure of the human kinematic model.

The structure of the paper is as follows. Section 2 presents a brief review of the dexterity measures which are used to evaluate the 6-REXOS. The design of the 6-REXOS is presented in section 3. Kinematic analysis is carried out to verify the effect of redundancy in the 6-REXOS and the details are presented in section 4. The proposed kinematic model of the human lower arm is presented in section 5. The last section is dedicated to the conclusion.

2. Review on dexterity measures

Kinematic redundancy in the 6-REXOS is verified based on dexterity measures, such as manipulability index [21], minimum singular value [21], condition number [22] and manipulability ellipsoids [23]. A brief summary of each measure is presented below.

2.1 Manipulability index

The manipulability index of a serial-link robotic manipulator depends on the Jacobian of the robot. Since the Jacobian is a joint configured parameter, the manipulability index varies with the joint space configuration [21]. The manipulability index for a redundant manipulator is given by equation (1):

$$w = \sqrt{\det(J.J^T)} \tag{1}$$

where w is the manipulability index, J is the Jacobian of the robot, and J^T is the transpose of the Jacobian. In general, a higher manipulability index shows better dexterous manipulation, while a lower value corresponds to limited manipulation [21]. Redundancy has the effect of improving the manipulability index [24]. The performance of the kinematic chain of the exoskeleton robot based on the manipulability index has rarely been addressed in the literature. However, the manipulability index is sometimes used to identify the performance of some exoskeleton robots (e.g., RiceWrist exoskeleton [25]).

2.2 Minimum singular value

Singular values of the Jacobian matrix are given by singular value decomposition (SVD), and the resulting singular matrix (Σ) (see equation 2) gives all singular values in its main diagonal. The minimum value in the main diagonal is taken as the minimum singular value (i.e., σ_m in equation 2).

$$\Sigma = \begin{bmatrix} \sigma_1 & & & 0 \\ & \sigma_2 & & \\ & & . & \\ & & & . \\ 0 & & & \sigma_m \end{bmatrix} \tag{2}$$

The minimum singular value indicates the closeness to singularity and at singular locations the manipulation is limited. Therefore, a higher minimum singular value shows dexterous manipulation [21]. Furthermore, redundancy has the effect of increasing the minimum singular value of a serial-link manipulator [22].

2.3 Condition number and manipulability ellipsoids

The condition number is a ratio between the largest singular value to the smallest singular value [22]. Dexterous manipulation in Cartesian space can be identified by using the condition number [22]. A low condition number points towards isotropic manipulation [26]. The redundancy reduces the condition number of a serial-link manipulator.

The numerical value of the manipulability index shows the volume of the manipulability ellipsoid [23]. The manipulability ellipsoid can then be used to visualize the manipulation in Cartesian space. Manipulability ellipsoid-based analysis of the kinematic chain of an exoskeleton robot is presented in [27].

3. 6-REXOS: Description of the design

The 6-REXOS has three motion-generating units: the elbow motion unit, the forearm motion unit and the wrist motion unit (see Fig. 2). The robot is designed to be worn on a human right hand, and can be attached to the wheelchair of a physically weak person through a passive shoulder joint. Two flexible bellow couplings are attached to the wrist and elbow units of the 6-REXOS. The kinematic redundancy is enhanced using flexible bellow couplings positioned at the wrist and elbow joints (see Fig. 2). The motion in the translational direction of each flexible bellow coupling has a passive DoF. In the human lower arm, the elbow joint and the wrist joint are two critical locations where joint axes misalignment can occur. The misalignments that can occur with the flexible bellow coupling (see Fig. 3) can reduce the kinematic mismatch between the human joint and the robot joint at elbow and wrist joints. As a result, the flexible bellow couplings attached into the 6-REXOS can improve kinematic redundancy and minimize kinematic discrepancies due to joint axes misalignment. A detailed description of each motion unit of the 6-REXOS is elaborated in subsequent sub-sections, and the joint configuration of the robot is presented in section 4.

3.1 Elbow motion unit

One of the bellow couplings is connected at the elbow joint of the 6-REXOS. The distal hub of the coupling is press-fitted with the distal link of the robot to reduce angular and parallel misalignments of the coupling (see Fig. 4-b). The motor shaft is connected to the hub of the bellow coupling, and the proximal hub of the bellow is mounted to the bearing, which is placed at the fixed link (see Fig. 4-b). The elbow flexion-extension motor (RSF-11B, Harmonic Drive

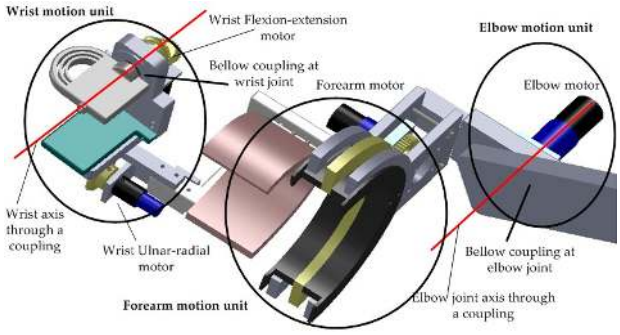

Figure 2. The 6-REXOS with main motion units

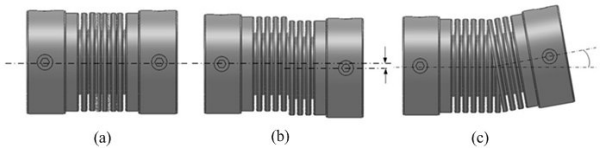

Figure 3. Types of misalignment in flexible bellow coupling: (a) axial, (b) parallel, (c) angular

Inc.) is attached to the 6-REXOS through a motor support plate. The motor rotates the distal link around the axis, passing through a bellow coupling. This motion generates the elbow flexion-extension (see Fig. 4-a). Compliance of the coupling helps to decouple the inertia from the actuator. The coupling at the elbow joint then achieves low inertia, which is a fundamental requirement for motion assistance.

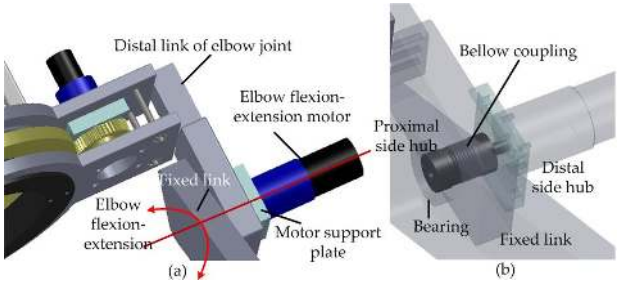

Figure 4. Elbow motion unit of the 6-REXOS

3.2 Forearm motion unit

A semi-circular open arm configuration is used for forearm supination-pronation, facilitating the wear of the 6-REXOS. The forearm motion is generated by sliding the guide plate through a semi-circular groove of the stationary plate (see Fig. 5-a). The semi-circular groove facilitates the forearm motion (see Fig. 5-a). The driven spur gear is placed in between two guide plates and the entire assembly is fixed to the forearm fixed plate using two bolts. In addition, one bolt is passed through a semi-circular groove. The proposed sliding mechanism in the 6-REXOS eliminates the need for an additional bearing. Thus, the weight of the 6-REXOS is reduced. The forearm motor (RSF-8B, harmonic drive Inc.) is positioned in the ulnar side and is attached to the 6-REXOS through a motor support plate (see Fig. 5-b).

The forearm motor rotates the driven spur gear at the forearm joint. This rotational motion about the forearm axis generates the supination-pronation of the 6-REXOS (see Fig. 5-a).

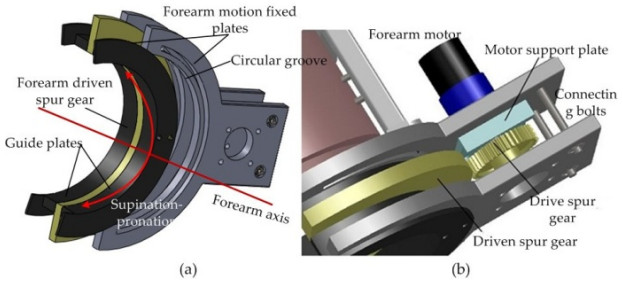

Figure 5. Forearm motion unit of the 6-REXOS

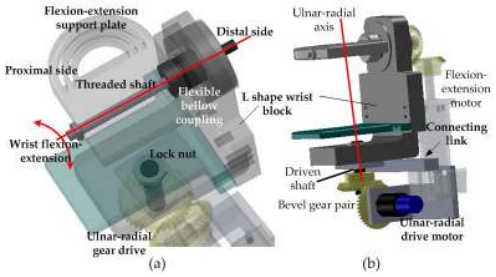

Figure 6. Wrist flexion-extension and ulnar-radial motion units

3.3 Wrist motion unit

The two wrist motions of flexion-extension and ulnar-radial deviation are generated at the L-shaped wrist block of the 6-REXOS, as shown in Figure 6. The second flexible bellow coupling is attached to the wrist flexion-extension axis (see Fig. 6-a). The distal hub of the coupling is connected to the driven shaft of the bevel gear, whereas the proximal hub is connected to the flexion-extension support plate through a threaded shaft and a lock nut. Several semi-circular grooves are produced on top of the flexion-extension support plate (see Fig. 6-a) to reduce the weight of support plate. The wrist flexion-extension motor (RSF-8B, Harmonic Drive Inc.) is placed at the ulnar side of the 6-REXOS and it is attached to the L-shaped wrist block using a motor support plate (see Fig. 6-b). The rotary motion of the motor is transferred to the flexion-extension support plate through a pair of bevel gears. Since the driven shaft of the bevel gear is connected to the bellow coupling, the rotational motion of the bellow about the flexion-extension axis generates the wrist flexion-extension (see Fig. 6-a).

The motor (RSF-8B, Harmonic Drive Inc.) of the wrist ulnar-radial deviation is connected to the L-shaped wrist block. A bevel gear pair is used to transmit the motion from the motor to the robot (see Fig. 6-b). The driven shaft of the bevel gear is firmly fixed to the L-shaped wrist block through a lock nut (see Fig. 7-a). The rotational motion

about the axis passes through a lock nut, generating the wrist ulnar-radial deviation (see Fig. 7-a).

According to the anatomy of the human wrist, the offset is observed between the two rotational axes [28]. Therefore, the wrist motion unit of the 6-REXOS is carefully designed considering the axes offset. In particular, a 5 mm offset is included between wrist flexion-extension and ulnar-radial deviation axes to promote comfort during manipulation of the 6-REXOS (see Fig. 7-b).

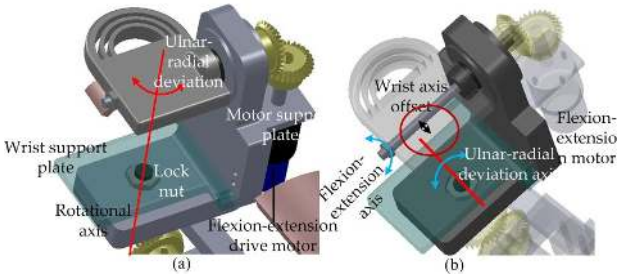

Figure 7. Wrist ulnar-radial deviation and axes offset

Specification	Elbow unit	Forearm unit	Wrist unit
Max: torque (Nm)	8.3	3.3	1.8
Max: speed (rev/min)	120	120	200
Max: current (A)	15.8	3.9	3.8
Inertia (kgm^2)	0.49x10^{-2}	0.16x10^{-2}	0.06x10^{-2}
Mass (kg)	0.5	0.3	0.3

Table 1. Specification of motors used in the 6-REXOS

Specification	Wrist joint	Elbow joint
Bore diameter (mm)	6	12
Outer diameter (mm)	20	47
Max. torque (Nm)	1.6	24
Moment of inertia (kgm^2)	9.9×10^{-7}	73.9×10^{-8}
Max. parallel offset (mm)	0.15	1
Max. angular offset (deg)	2	1
Max. axial displacement (mm)	2	2

Table 2. Specifications of flexible bellow couplings

3.4 Actuation of the 6-REXOS

The motion units of the 6-REXOS are actuated by DC motors. Inertia and weight of the human lower arm are taken into account to calculate joint torques. The bandwidth and power-to-weight ratio are also considered during the motor selection. The specifications of the motors used in the 6-REXOS are presented in Table 1.

Three motors are placed at the ulnar side of the 6-REXOS and the wrist ulnar-radial deviation motor is placed in the base of the L-shaped wrist block. Thus, the motors do not disturb the wearer's performance of daily activities. The specifications of the flexible bellow couplings used in the 6-REXOS are given in Table 2. Features such as low inertia, high stiffness, low weight and zero backlash motivate the use of the selected flexible bellow coupling.

4. Kinematic analysis of the 6-REXOS

Kinematic analysis is carried out to study the effect of redundancy caused by adding passive translational motion at the wrist and elbow joints (i.e., adding two flexible bellow couplings) of the 6-REXOS. A kinematic chain is defined for the 6-REXOS and another kinematic chain is defined with four DoFs, derived by neglecting the contribution of two flexible bellow couplings in the 6-REXOS. The four-DoF robot with the four-DoF kinematic chain is similar to most of the lower-arm kinematic chains explored in the literature [25]. Therefore, the four-DoF kinematic robot can be used to compare the performance of the 6-REXOS with other lower-arm exoskeleton robots.

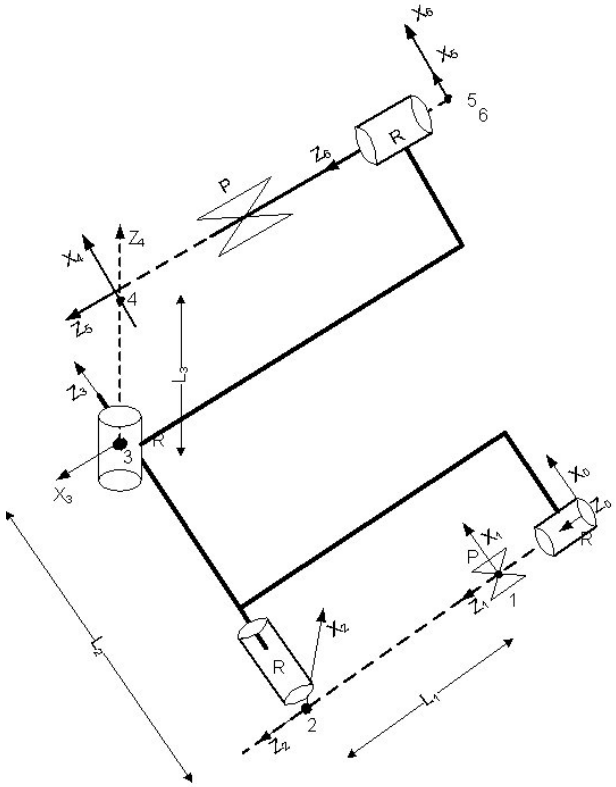

Figure 8. D-H frame assignment for the 6-REXOS. P: Prismatic joint, R: Revolute joint.

The degree of manipulation is an important measure since the 6-REXOS is used for daily motion assistance. Therefore, manipulability index and condition number are used to identify the dexterous manipulation of the 6-REXOS in the reachable workspace. Furthermore, the minimum singular value is used to understand the effect of singularity due to kinematic redundancy. Manipulability ellipsoids are used to visualize the manipulation in operational space. Simu-

lation as well as kinematic analysis of the 6-REXOS are performed using Robotics Toolbox (RTB) [29] running on Matlab.

4.1 Frame assignment of the 6-REXOS

Denevit-Hartenberge (D-H) notation is used to define the link frames of the 6-REXOS (see Fig. 8). In Figure 8, 'P' stands for prismatic joint of flexible bellow couplings and 'R' stands for revolute joint. Z_0 indicates the fixed base and Z_1 defines the joint axis at elbow translational joint. The rotational axis of elbow flexion-extension is defined in the Z_2 direction. Z_3 defines the rotational axis of forearm supination-pronation. Wrist ulnar-radial deviation axis is defined in the Z_4 direction and wrist translational DoF is defined from the Z_5 axis. Z_6 is used to define the wrist flexion-extension axis.

i	α_{i-1}	a_{i-1}	d_i	θ_i
1	0^0	0	d_1	-
2	0^0	0	L_1	θ_2
3	-90^0	0	L_2	θ_3
4	-90^0	0	L_3	θ_4
5	-90^0	a_3 (offset)	d_2	-
6	0^0	0	0	θ_6

Table 3. D-H table for the 6-REXOS

D-H parameters of the 6-REXOS are given in Table 3. In Table 3, θ_2, θ_3, θ_4 and θ_6 are elbow angle, forearm angle, wrist ulnar-radial deviation angle and wrist flexion-extension angle, respectively.

A transformation matrix between two consecutive joint axes is calculated from the transformation matrix given in equation (3).

$$ {}^{i-1}_{i}T = \begin{bmatrix} c\theta_i & -s\theta_i & 0 & a_{i-1} \\ s\theta_i c\alpha_{i-1} & c\theta_i c\alpha_{i-1} & -s\alpha_{i-1} & -s\alpha_{i-1}d_i \\ s\theta_i s\alpha_{i-1} & c\theta_i s\alpha_{i-1} & c\alpha_{i-1} & c\alpha_{i-1}d_i \\ 0 & 0 & 0 & 1 \end{bmatrix} \quad (3) $$

where 'c' stands for the cosine and 's' stands for the sine of angles of rotation.

The forward transformation matrix is evaluated from base frame (frame 0) to end-effector frame (frame 6) using equation (4):

$$ {}^{0}_{6}T = {}^{0}_{1}T\,{}^{1}_{2}T\,{}^{2}_{3}T\,{}^{3}_{4}T\,{}^{4}_{5}T\,{}^{5}_{6}T \quad (4) $$

Since dexterity measures depend on the Jacobian matrix, the Jacobian of the 6-REXOS is derived using equation (5). Each column of the Jacobian matrix represents the joint space. The top row represents the translation part and the bottom row represents the rotational part. Since the first and fifth joints of the 6-REXOS are prismatic joints, the rotational part of

$$ J = \begin{bmatrix} Z_1^0 & \frac{\partial x_p}{\partial q_2} & \frac{\partial x_p}{\partial q_3} & \frac{\partial x_p}{\partial q_4} & Z_5^0 & \frac{\partial x_p}{\partial q_6} \\ 0 & Z_2^0 & Z_3^0 & Z_4^0 & 0 & Z_6^0 \end{bmatrix} \quad (5) $$

the Jacobian is equal to a zero vector (see equation 5). Furthermore, the position vector (x_p) of the end-effector with reference to the base frame is given by equation (6):

$$ x_P = \begin{bmatrix} L_2 s_2 + a_3(s_2 s_4 + c_2 c_3 c_4) - d_5(c_4 s_2 - c_2 c_3 s_4) + L_3 c_2 s_3 \\ L_2 c_2 + a_3(c_2 s_4 - c_3 c_4 s_2) - d_5(c_2 c_4 + c_3 s_2 s_4) - L_3 s_2 s_3 \\ L_1 + d_1 - L_1 c_3 + a_3 c_4 s_3 + d_5 s_3 s_4 \end{bmatrix} \quad (6) $$

where L_1, L_2 and L_3 are link lengths; c_i (i=2,3,4) is the cosine of the joint angle; s_i (i=2,3,4) is the sine of the joint angle, and d_1 and d_5 are prismatic joint parameters.

The joint trajectory for the 6-REXOS is defined between two joint configurations as shown in Figure 9. The initial joint pose is taken as d_1= 0, θ_2 = -π/18, θ_3 = -π/3, θ_4 = -π/6, d_5 = 0, θ_6 = -π/3 and the final joint pose is taken as d_1= 2, θ_2 = 2π/18, θ_3 = π/3, θ_4 = π/6, d_5 = 2, θ_6 = π/3. Joint trajectory is generated (see Fig. 9) using Robotics Toolbox and divided into 20 sample points. The Jacobian of the 6-REXOS is calculated numerically at each joint configuration.

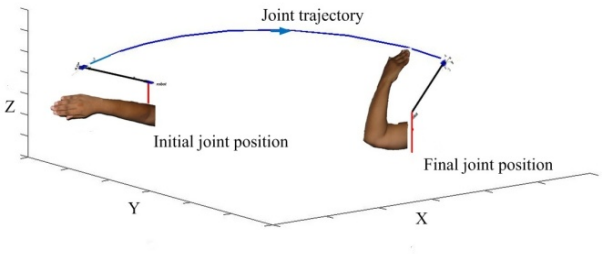

Figure 9. Defined joint trajectory of the 6-REXOS

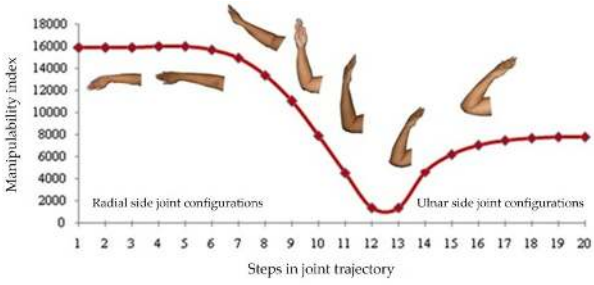

Figure 10. Manipulability variation of the 6-REXOS. Lower arm positions related to joint configurations are also shown.

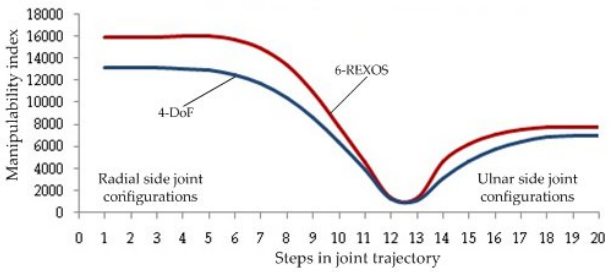

Figure 11. Comparison of manipulability variation

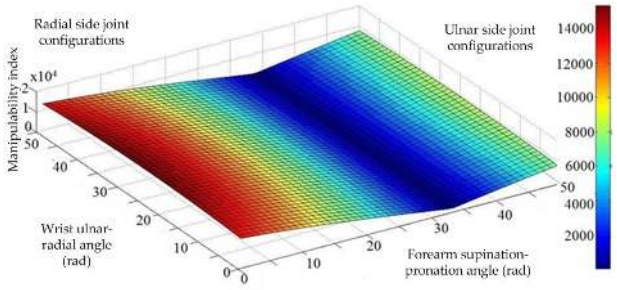

Figure 12. Variation of manipulability index of four-DoF robot

4.2 Manipulability index

The Jacobian as well as its transpose is calculated at each joint position and the calculation is continued to all 20 steps in the joint trajectory of the 6-REXOS. Finally, the manipulability index of each step is determined using equation (1). The variation of the manipulability index over the joint trajectory is shown in Figure 10. Configurations of the human lower arm throughout the joint trajectory are also shown in the same figure. According to the result, the 6-REXOS shows a higher manipulability index in the radial-side joint trajectory than on the ulnar side. Since the 6-REXOS is designed to be worn on the human right hand, radial-side manipulability is more significant than ulnar-side manipulability to perform daily tasks. The manipulability variation for the four-DoF robot is determined following the same procedure. Variation of manipulability indices for two kinematic chains is given in Figure 11. It can be seen that the manipulability index of the 6-REXOS is higher than the four-DoF robot as a result of kinematic redundancy. This improvement affects the radial side as well as the ulnar side of the joint trajectory. The minimum manipulability region is observed in the 10^{th} to 14^{th} steps of the joint trajectory (see Fig. 11). However, the non-zero manipulability index in the 12^{th} to 13^{th} steps indicates the non-existence of singularity in both exoskeleton robots. Calculation of manipulability index is extended to the entire workspace in order to visualize the whole variation. The translational Jacobian of two exoskeleton robots (i.e., 6-REXOS and four-DoF robot) is evaluated symbolically using Matlab. Symbolic expressions of manipulability indices are used to visualize the variation of manipulability index. Variations of manipulability index of the four-DoF robot and the 6-REXOS are given in Figure 12 and Figure 13, respectively. Redundancy in the 6-REXOS alters the manipulability index variation in the radial-side as well as in the ulnar-side joint trajectory, as compared to the four-DoF robot. Furthermore, radial-side manipulability is improved and minimum manipulability region is shifted to the ulnar side of the joint trajectory in the 6-REXOS (see Fig. 13). Since ulnar-side joint trajectory contributes less to daily activities, shifting the minimum manipulability region to the ulnar side does not degrade the ability to perform daily tasks.

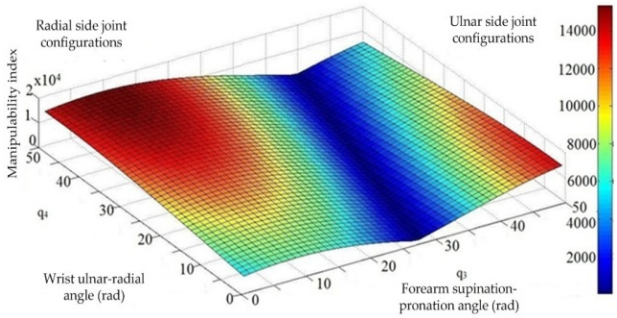

Figure 13. Manipulability index of the 6-REXOS

4.3 Minimum singular value

Singular value decomposition (SVD) is applied to the Jacobian of the 6-REXOS as well as the four-DoF exoskeleton robot. The resulting singular matrix (Σ) gives all singular values in its main diagonal. The minimum is taken as the minimum singular value of the kinematic chain. Moreover, the minimum singular values of the 6-REXOS and the four-DoF exoskeleton robot are used to determine minimum manipulability regions in the joint trajectory. The variations of singular values are shown in Figure 14. The 6-REXOS shows a larger minimum singular value than the four-DoF exoskeleton robot (see Fig. 14). The 6-REXOS is capable of maintaining a larger minimum singular value throughout the joint space. Since the minimum singular value indicates the closeness to singularity, the higher minimum singular value in the 6-REXOS verifies the higher distance to the singular locations. This indicates that the degree of manipulation is improved in the 6-REXOS due to its redundancy.

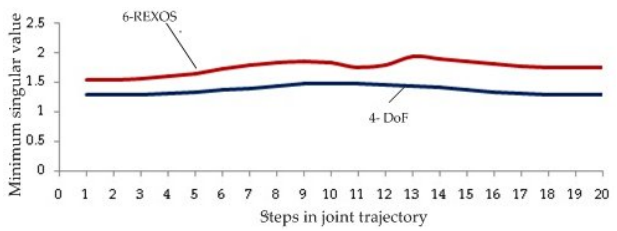

Figure 14. Comparison of the minimum singular value

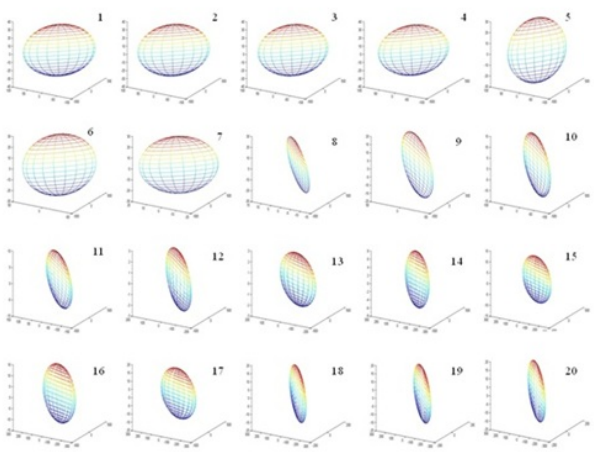

Figure 15. Manipulability ellipsoids for the four-DoF robot (superscript shows the step of the joint trajectory)

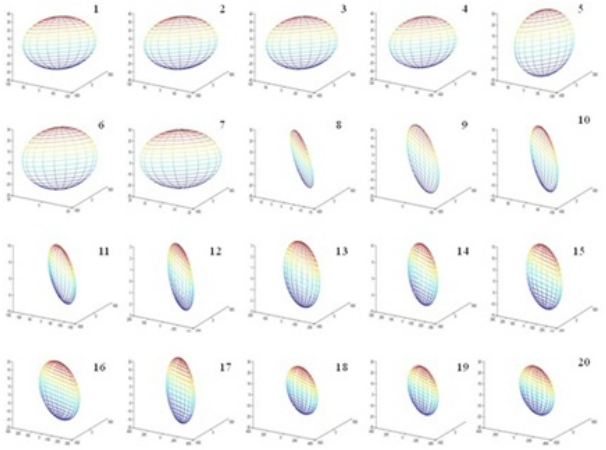

Figure 16. Manipulability ellipsoids for the 6-REXOS (superscript shows the step of the joint trajectory)

4.4 Manipulability ellipsoid

Since the manipulability index is proportional to the volume of the manipulability ellipsoid, it can be used to visualize the degree of manipulation in the operational space. Therefore, the manipulability ellipsoids are constructed based on the Jacobian and its singular values. The RTB function 'plot_ellipse' with the Jacobian at the relevant joint configuration is used to obtain the ellipsoids corresponding to each step of the joint trajectory. This method is applied to the 6-REXOS as well as the four-DoF robot. The 3D view of the manipulability ellipsoids for the four-DoF robot is given in Figure 15. Manipulability ellipsoids related to the initial joint steps (see steps 1 to 7 in Fig. 15) of the joint trajectory show a greater span in Cartesian directions. This indicates that the four-DoF robot has good manipulation in operational space. However, when it passes through the minimum manipulability region, the manipulability ellipsoids (see steps 8 to 12 in Fig. 15) have limited and restricted manipulation in operational space. Again, manipulability ellipsoids corresponding to ulnar-side joint configurations (see step 13 onwards in Fig. 15) also show limited manipulation in operational space. In general, limited manipulation in operational space is not a desirable outcome for the motion assistance since it can induce discomfort to the wearer during the motion. Manipulability ellipsoids for the 6-REXOS are given in Figure 16.

Manipulability ellipsoids of the 6-REXOS show an improvement in Cartesian directions as compared to the four-DoF robot. Manipulation of the 6- REXOS is distributed in Cartesian directions, which is the same as for the four-DoF robot in the initial joint steps. However, a more spherical form for the manipulability ellipsoids can be seen for the 6-REXOS. This is significant in the minimum manipulability region as well as in the ulnar side (see beyond step 13 in Fig. 16). This implies that redundancy in the 6-REXOS comprises a positive trend to improve the level of manipulation in the operational space. This is a desirable feature with respect to the wearer's point of view since comfort during the manipulation is essential for the motion assistance.

4.5 Condition number

Condition number is determined for the exoskeleton kinematic chains to identify the dexterous manipulation in the task space. SVD generates a singular matrix (Σ) for the Jacobian. The first diagonal element corresponds to the largest singular value while the lowest diagonal element refers to the minimum singular value. Variation of manipulability ellipsoids can be seen in an analysis of the condition number. Based on the singular values of the Jacobian of the four-DoF robot and the 6-REXOS, the condition numbers for two exoskeleton robots are separately calculated. The 6-REXOS has a low condition number compared to the four-DoF exoskeleton robot (see Fig. 17). Since the main axis of an ellipsoid is given by a singular value, a low condition number indicates a more spherical form for a manipulability ellipsoid. This implies that the degree of manipulation is uniformly distributed to all Cartesian directions in the operational space. This verifies the capability of providing uniform manipulation in the task space due to the kinematic redundancy in the 6-REXOS.

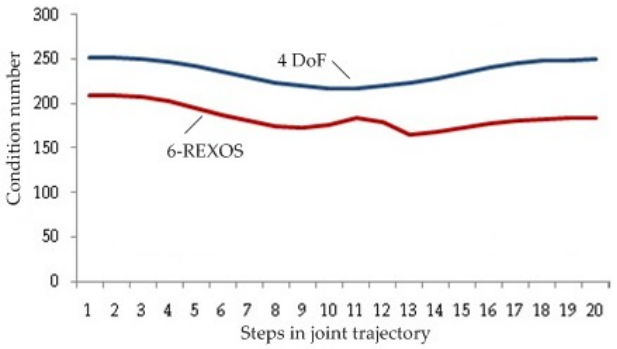

Figure 17. Comparison of condition number

5. Kinematic model of human lower arm

A kinematic model of the human lower arm is required to validate/benchmark the proposed 6-REXOS. Therefore, a kinematic model is proposed for the human lower arm in order to identify the effectiveness of embedding kinematic redundancy into the 6-REXOS. However, developing an exact kinematic model for a human upper limb is not an easy task due to the complexities of the human anatomy and the subject-dependency of relevant parameters. Nevertheless, several kinematic models have been proposed for human upper limbs in the literature. A seven-DoF kinematic model is proposed in [30] and in [31]. Furthermore, a nine-DoF kinematic model is proposed for a human upper limb with complexity at the shoulder joint. Additionally, an upper-limb kinematic model with 10 DoFs is proposed in [32]. In contrast to the DoFs in the human upper limb, many models use a four-DoF kinematic model for the human lower arm, such as the lower arm of CADEN-7 [30]. For example, Malek et al. [31]and Chan et al. [32] show a four-DoF model for lower arm. The human wrist comprises a complex anatomical structure. Typically, two DoFs are associated with the human wrist: flexion-extension and ulnar-radial deviation [28]. Furthermore, the wrist flexion-extension axis passes through the head of the capitate [28].

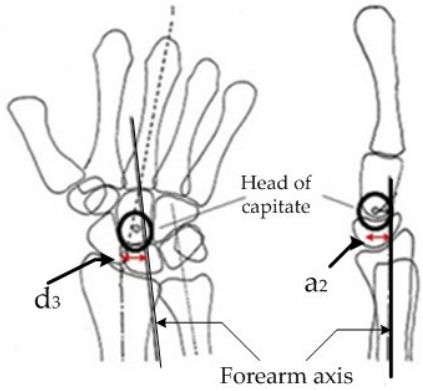

Figure 18. Deviations of head of capitate on forearm axis

i	α_{i-1} (deg)	a_{i-1} (mm)	d_i (mm)	θ_i	Initial pose (deg)	Final pose (deg)
1	0^0	0	0	θ_1	0	140
2	-90^0	0	250	θ_2	-60^0	60^0
3	90^0	a_2	d_3	θ_3	-60^0	60^0
4	90^0	8	0	θ_4	-35^0	35^0

Table 4. D-H table for human lower arm

According to [28], the head of capitate does not coincide with the forearm axis. Deviations are shown from the forearm axis (taken as d_3) as well as the plane which passes through the forearm axis (taken as a_2) (see Fig. 18 [28]). These deviations have not been considered for the human upper-limb kinematic models proposed in the literature. Therefore, a four-DoF kinematic model is proposed for human lower arm considering those deviations. The modified D-H notation is used for the frame assignment (see Fig. 19). Elbow flexion-extension is taken about the Z_1 axis. Z_2 defines forearm supination-pronation axis while Z_3 defines wrist flexion-extension axis. Wrist ulnar-radial deviation is taken about the Z_4 direction. The average forearm length is taken as 250 mm and the average wrist axis offset is taken as 8 mm. The average deviation of the head of capitate with respect to the forearm axis is taken as d_3 (= 1.5 mm) and the average deviation from the forearm plane is taken as a_2 (= 0.646 mm). The D-H table for the proposed human-lower-arm model is given as Table 4.

The joint space of the proposed kinematic model is simulated using RTB in order to compare the range of motions of the proposed model with the range of human motions. The result shown in Figure 20 shows that the range of motions of the proposed model is approximately the same as the range of human motions. Typically the positions of wrist axes are not unique and vary from person to person. In the literature, a typical value of a_2 is defined as 0.01 times the length of the third meta-carpal bone [28], and the value of d_3 is defined as one-twelfth of the distance between the radial and ulnar axes of the forearm [28]. Furthermore, the length of the third metacarpal bone and the distance between the radial and ulnar axes varies from person to person. Therefore, the range for a_2 is taken as 0.01 × (64.60 ± 5.38) mm [33] while d_3 is taken as (1.5 ± 0.25) mm [28]. Since the 6-REXOS is designed for the daily motion assistance of physically weak people, the dependency of the manipulability index of the human kinematic model is investigated against wrist parameters a_2 and d_3. For this, the available range of a_2 and d_3 is varied by 25% from the upper limit as well as from the lower limit. The values corresponding to each percentage of d_3 and a_2 are given in Table 5. The joint trajectory for the human kinematic model is generated in between the initial pose and the final pose (see Table 4) and 20 sample points are defined in the generated joint trajectory. Variation of manipulability index for different wrist parameters is evaluated based on the sensitivity analysis. In order to investigate the variation of manipulability index for the change of d_3, a_2 is kept as constant at its average value (0.646 mm) and d_3 is varied from 1.75 mm to 1.5 mm. A manipulability index is calculated for each value of d_3 and plotted as shown in Figure 21. The same calculation procedure is repeated to investigate the variation of manipulability index change for different values of a_2. In this case, d_3 is kept as constant at its average value (1.5 mm) and a_2 is varied from 0.699 mm to 0.592 mm. The variation of manipulability index

change for different a_2 values is plotted in Figure 22. The result shown in Figure 21 shows that increasing the distance to the head of capitate on the forearm axis in the radial direction (for the right hand) improves the manipulability index in the radial-side joint trajectory. Moreover, the change of a_2 contributes to altering the manipulability index in the ulnar-side joint trajectory, whereas the manipulability index change is the minimum on the radial-side joint trajectory (see Fig. 22). Since the 6-REXOS is designed to be worn on the human right hand, radial-side manipulation is more important than ulnar-side manipulation to perform daily activities. The distance d_3 is associated with the position of head of capitate in the radial direction in the human right hand (see Fig. 18). Higher d_3 improves the manipulation of the human-lower-arm model. Therefore, it is important to incorporate a mechanism into an exoskeleton robot that improves the motion in the ulnar-radial deviation of the right hand. In fact, the compliance of flexible bellow coupling placed at the flexion-extension axis of the wrist joint of the 6-REXOS can be used to provide passive motion to improve the manipulation in the ulnar-radial direction. Figure 23 illustrates the effect of passive compliance of the flexible bellow coupling to improve the manipulation in the ulnar-radial direction. The double-headed straight arrow shows the passive linear motion of the flexible bellow coupling along the flexion-extension axis. The curved arrow shows the ulnar-radial deviation. When the wearer performs ulnar-radial deviation, the passive DoF at the flexible bellow coupling promotes the motion in the radial direction. This improves the manipulation of the 6-REXOS.

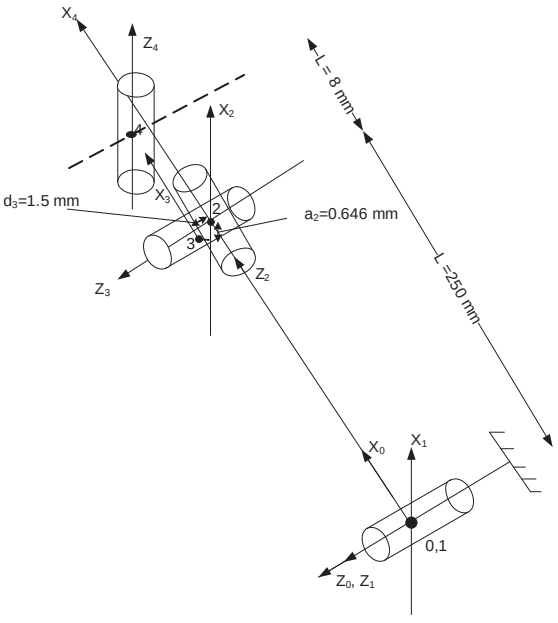

Figure 19. Proposed kinematic model for human lower arm

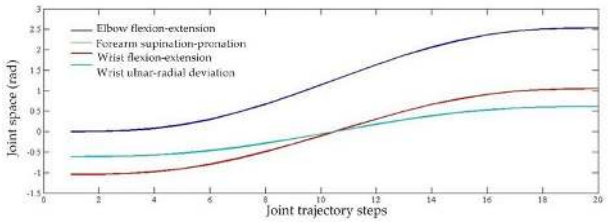

Figure 20. Range of motion for proposed human lower arm model

Percentage (%)	a_2 (mm)	d_3 (mm)
100(upper limit)	0.699	1.75
75	0.686	1.687
50	0.673	1.625
25	0.659	1.563
0 (average)	0.646	1.5
-25	0.632	1.437
-50	0.619	1.375
-75	0.606	1.312
-100 (lower limit)	0.592	1.5

Table 5. Percentage variations of d_3 and a_2

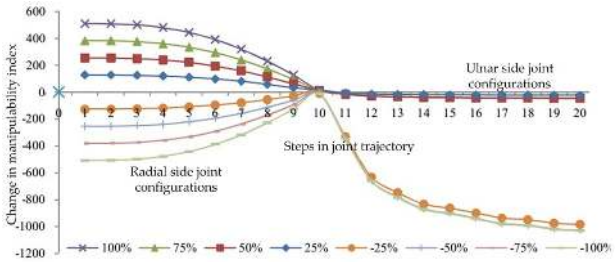

Figure 21. Change of manipulability index against to d_3

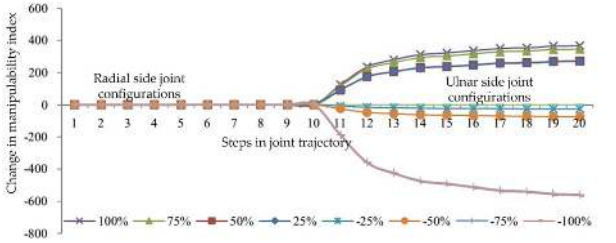

Figure 22. Change of manipulability index against to a_2

The manipulability index of the lower arm model is used to investigate the effectiveness of redundancy of the 6-REXOS. The manipulability index of the 6-REXOS, the four-DoF exoskeleton robot and the proposed lower arm model are plotted in the same graph to visualize the variations relative to each other (see Fig. 24). Three regions are identified – A, B and C in Figure 24. In region A, the manipulability index of the four-DoF robot is lower than for the other two cases and the 6-REXOS has a manipula-

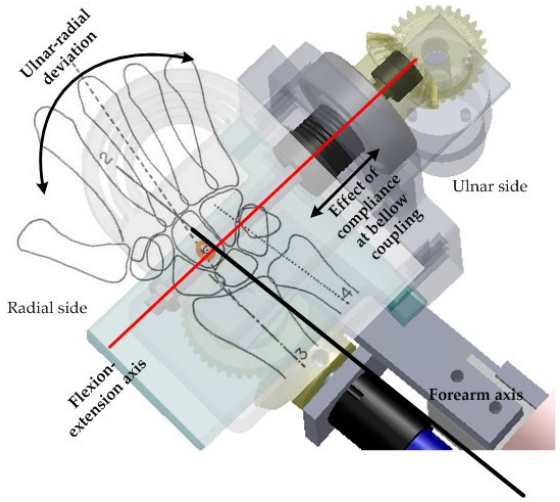

Figure 23. Effect of passive compliance at wrist joint of the 6-REXOS

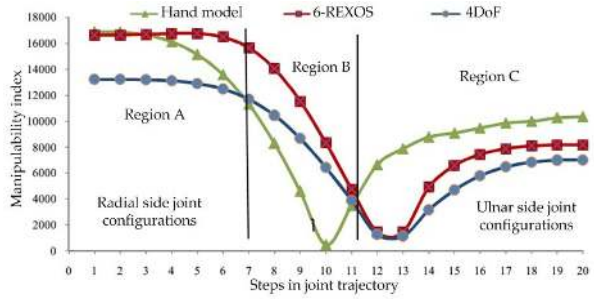

Figure 24. Comparison of manipulability indices

bility index on a par with the lower arm model for initial joint positions in the radial side. The manipulability index of the lower arm model shows a lower value than both exoskeleton robots in region B. Furthermore, the manipulability index of the lower arm model is higher in region C than in the two exoskeleton robots. However, a drop in the manipulability index in region C is not highly significant, because the ulnar-side joint trajectory shows a lower contribution to the performance of daily activities with the right hand. Since radial-side manipulability is important for the right-hand manipulation, the 6-REXOS has a higher manipulability index than the hand model in the radial-side joint trajectory. Therefore, it can be concluded that adding kinematic redundancy to the 6-REXOS through a flexible bellow coupling improves the manipulation. This is an important result to guarantee the comfort of the motion assistance of the 6-REXOS.

6. Conclusion

This paper has proposed a six-DoF upper-limb exoskeleton robot (6-REXOS) for the motion assistance of physically weak people, considering kinematic redundancy and passive compliance to improve the pHRI. The proposed 6-REXOS used two passive DoFs through two flexible bellow couplings. These couplings were positioned in the kinematic chain of the 6-REXOS to ensure kinematic redundancy. The effect of kinematic redundancy was verified based on dexterity measures such as manipulability index, minimum singular value, condition number and manipulability ellipsoids. An exoskeleton robot with a four-DoF kinematic chain was presented to compare the performance of the 6-REXOS. The kinematic redundancy of the 6-REXOS improved the maximum manipulability index by 21.13%, while the minimum index was improved by 22.25% compared with the four-DoF robot.

A kinematic model was proposed for the human lower arm considering variations of the human wrist parameters. The manipulability of the lower arm model was investigated by varying human wrist parameters to identify the contribution for manipulability variation. The significance of the compliance gained from the bellow coupling at the wrist joint of the 6-REXOS was identified based on the manipulability index of the lower arm model. Furthermore, the manipulability index of the proposed lower arm model was used to verify the performance of the 6-REXOS. It can be concluded that adding kinematic redundancy to the 6-REXOS through a flexible bellow coupling improves its manipulation. This ensured the quality of pHRI was improved in the upper-limb exoskeleton.

7. Acknowledgements

The authors would like to acknowledge the support given by National Research Council of Sri Lanka through a research grant (grant no: 11-067).

8. References

[1] H. S. Lo and S. Q. Xie, "Exoskeleton robots for upper-limb rehabilitation: State of the art and future prospects," Medical Engineering and Physics, vol. 34, no. 3, 2012, p. 261–268.

[2] J. Rosen and J. C. Perry, "Upper Limb Powered Exoskeleton," International Journal of Humanoid Robotics, vol. 4, no. 3, 2007, p. 529–548.

[3] J. L. Pons, Ed., Wearable Robots: Biomechatronic Exoskeletons. John Wiley & Sons, Ltd., 2008.

[4] P. Martin and M. R. Emami, "Neuro-fuzzy Compliance Control for Rehabilitation Robotics," in 3rd IEEE RAS & EMBS International Conference on Biomedical Robotics and Biomechatronics, 2010, p. 560–565.

[5] K. Kiguchi, M. H. Rahman, and M. Sasaki, "Neuro-Fuzzy based Motion Control of a Robotic Exoskeleton: Considering End-effector Force Vectors," in IEEE International Conference on Robotics and Automation, 2006, p. 3146–3151.

[6] M. H. Rahman, T. K. Ouimet, M. Saad, J. P. Kenne, and P. S. Archambault, "Development of a 4 DoFs Exoskeleton Robot for Passive Arm Movement

Assistance," International Journal of Mechatronics and Automation, vol. 2, no. 1, 2012, p. 34–50.

[7] W. Yu and J. Rosen, "Neural PID Control of Robot Manipulators With Application to an Upper Limb Exoskeleton," IEEE Transactions on Cybernetics, vol. 43, no. 2, 2013, p. 673–684.

[8] M. Mihelj, "Human Arm Kinematics for Robot Based Rehabilitation," Robotica, vol. 24, no. 03, 2006, p. 377–383.

[9] R. A. R. C. Gopura, K. Kiguchi, and Y. Li, "SUEFUL-7: A 7 DoF Upper-Limb Exoskeleton Robot with Muscle-Model-Oriented EMG-Based Control," in IEEE/RSJ International Conference on Intelligent Robots and Systems, 2009, p. 1126–1131.

[10] B. Tondu, "A Theorem on the Manipulability of Redundant Serial Kinematic Chains," Electrical Engineering Dept., Campus de Rangueil, France, 2007.

[11] O. Khatib and B. Siciliano, Eds., Springer Handbook of Robotics. Springer, 2008.

[12] M. Esmaeili, K. Gamage, E. Tan, and D. Campolo, "Ergonomic Considerations for Anthropomorphic Wrist Exoskeletons: A Simulation Study on the Effects of Joint Misalignment," in IEEE/RSJ International Conference on Intelligent Robots and Systems, 2011, p. 4905–4910.

[13] A. Schiele, "Ergonomics of Exoskeletons: Subjective Performance Metrics," in IEEE/RSJ International Conference on Intelligent Robots and Systems, 2009, pp. 480–485.

[14] S. J. Ball, I. E. Brown, and S. H. Scott, "MEDARM: A Rehabilitation Robot with 5 DoF at the Shoulder Complex," in IEE/ASME International Conference on Advanced Intelligent Mechatronics, 2007, p. 25–30.

[15] K. Kiguchi and T. Fukuda, "Upper-Limb Exoskeletons for Physically Weak Persons," in Rehabilitation Robotics, S. S. Kommu, Ed. Intech Austria, 2007, p. 287–299.

[16] N. Vitiello, T. Lenzi, S. Roccella, S. Marco, M. De Rossi, E. Cattin, F. Giovacchini, F. Vecchi, and M. C. Carrozza, "NEUROExos: A Powered Elbow Exoskeleton for Physical Rehabilitation," IEEE Transactions on Robotics, vol. 29, no. 1, 2013, p. 220–235.

[17] D. Naidu, R. Stopforth, G. Bright, and S. Davrajh, "A Portable Passive Physiotherapeutic Exoskeleton," International Journal of Advanced Robotic Systems, vol. 9, no. 137, 2012, p. 1–12.

[18] L. Zollo, B. Siciliano, A. De Luca, E. Guglielmelli, and P. Dario, "Compliance Control for an Anthropomorphic Robot with Elastic Joints: Theory and Experiments," Journal of Dynamics Systems, Measurement and Control, vol. 127, no. 4, 2005, p. 321–328.

[19] G. Morel and N. Jarrasse, "Connecting a Human Limb to an Exoskeleton," IEEE Transactions on Robotics, vol. 28, no. 3, 2012, p. 697–709.

[20] S. Drive, "Stock drive products/Sterling instruments." [Online] Available: http://www.sdp-si.com, Accessed on 10 May 2013.

[21] T. Yoshikawa, "Manipulability of Robotic Mechanisms," The International Journal of Robotic Research, vol. 4, no. 3, 1985, p. 2–9.

[22] S. Siddiqui and R. Roberts, "An Example of a Fault Tolerant Wrist Design," in Florida Conference on Recent Advanced in Robotics, 2012, p. 1–4.

[23] T. Yoshioka, Foundation of Robotics: Analysis and Control, 2nd ed. MIT Press, Cambridge, USA, 2001.

[24] M. Mohammed, A. Elkady, and T. Sobh, "A New Algorithm for Measuring and Optimizing the Manipulability Index," International Journal of Advanced Robotic Systems, vol. 6, no. 2, 2009, p. 145–150.

[25] A. Gupta and M. K. O, Malley, "Design of a Haptic Arm Exoskeleton for Training and Rehabilitation," IEEE/ASME Transactions on Mechatronics, vol. 11, no. 3, 2006, p. 280–289.

[26] H. Abdi and S. Nahavandi, "Well-Conditioned Configurations of Fault-Tolerant Manipulators," Journal of Robotics and Autonomous Systems, vol. 60, no. 2, 2009, p. 242–251.

[27] H. Kim, L. M. Miller, N. Byl, G. M. Abrams, and J. Rosen, "Redundancy Resolution of the Human Arm and an Upper Limb Exoskeleton," IEEE Transactions on Biomedical Engineering, vol. 59, no. 6, 2012, p. 1770–1779.

[28] Y. Youm and A. Flatt, "Design of a Total Wrist Prosthesis," Annals of Biomedical Engineering, vol. 12, 1984, p. 247–262.

[29] P. I. Corke, "A robotic toolbox for MATLAB," IEEE Robotics and Automation Magazine, Sept. 1996, p. 24–32.

[30] J. C. Perry, J. Rosen, and S. Burns, "Upper-Limb Powered Exoskeleton Design," IEEE/ASME Transactions on Mechatronics, vol. 12, no. 4, 2007, p. 408–417.

[31] J. Yang, K. A. Malek, and K. Nebel, "Reach Envelop of A 9-Degree of Freedom Model of The Upper Extremity," International Journal of Robotics and Automation, vol. 20, no. 4, 2005, p. 240–259.

[32] M. F. Chan, D. R. Giddings, C. S. Chandler, C. Crags, R. D. Plant, and M. C. Day, "An Experimentally Confirmed Statistical Model on Arm Movement," Human Movement Science, vol. 22, no. 02, 2004, p. 631–648.

[33] A. Buryanov and V. Kotiuk, "Proportions of Hand Segments," International Journal of Morphol, vol. 28, no. 3, 2010, p. 755–758.